The Effect of Cell and Module Dimensions on Thermomechanical Stress in PV Modules

Andreas J. Beinert ⓘ, Pascal Romer, Martin Heinrich, Max Mittag, Jarir Aktaa, and D. Holger Neuhaus

Abstract—We present an evaluation of the silicon solar cell as well as the photovoltaic (PV) module size and its effect on thermomechanical stress. The evaluation is based on finite-element method (FEM) simulations. Within these simulations, we perform parameter variations of the number of solar cells within a PV module from 60–140 cells, of the cell size from 156.0–161.75 mm, and the cell format from full cells down to quarter cells. The FEM simulations cover the lamination process, mechanical load, and thermal cycling for glass–foil as well as glass–glass modules. The presented results reveal correlations between the solar cell and module size with the stress in the solar cells. We also find that the interaction of the laminate with the module frame plays a significant role in thermal cycling. Of the varitations under investigation, the increase in cell size has the largest effect on the stress. However, at a mechanical load of 2400 Pa, glass–foil modules with less than 96 solar cells have a negligible failure probability. The advantage of placing the solar cells in the neutral axis of the laminate is proven by the negligible tensile stress values for all variations of the glass–glass modules.

Index Terms—Finite-element analysis (FEM), FEM simulations, mechanical load, photovoltaic (PV) module, PV module size, solar cell size, stress, thermomechanics, thermal cycling, virtual prototyping.

I. INTRODUCTION

IN THE recent past, glass–foil photovoltaic (PV) modules with 60 solar cells have dominated the market. According to the tenth edition of the International Technology Roadmap for Photovoltaic (ITRPV) [1], the market might shift to larger modules, with 60-cell PV modules covering only about 40% in 2029. For the cell format, the ITRPV predicts a similar trend. In 2029, more than 40% of the PV modules could be made of cut cells, such as half cells or quarter cells. At the same time, the wafer size might shift away from the 156.0 mm edge length to larger wafers and the market share of glass–glass PV modules is supposed to increase. With PV module degradation rates of up to 8% relative power loss per year due to cell cracks [2] in conventional PV modules, the question about the effect of these predicted trends on the thermomechanical stress in the solar

Fig. 1. FEM model geometry of the reference module with the symmetry axes depicted (green lines). The orange rectangles show the position of the fixed constraint at 20% of the module length from the edge.

cells raises. The thermomechanics of conventional PV modules was investigated by various researchers using the finite-element method (FEM) [3]–[6]. According to the FEM simulation of Kraemer *et al.* [7], glass–glass modules show no bending in thermal cycling (TC), but the ribbons show higher compressive stress. Also, experimental investigations have been performed [8]–[12]. With this study, we add to the understanding of the thermomechanics of PV modules by investigating the predicted trends using the FEM simulations to analyze the effects of stress related to module testing according to IEC 61215 [13]. We benchmark potential new PV module designs versus a reference design (glass–foil with 60 full-square solar cells of 156.75 mm width). This is an extended evaluation of a study published elsewhere [14].

II. METHOD

We have built a 3-D FEM model using the commercial software Comsol Multiphysics version 5.4 of a standard PV module based on two validated models published previously [12], [15], [16]. Due to the large aspect ratio of the solar cell edge length to its thickness, mechanical modeling of PV modules is a challenging task. To minimize the computational effort, we exploit the twofold axial symmetry of the PV laminate, as shown in Fig. 1, by modeling a quarter laminate. As the metallization has no significant effect on the stress [17], we implement the solar cells as full-square monocrystalline silicon wafer without metallization. The maximum tensile stress from the solder joint occurs at the end of the busbar. For distances to

TABLE I
SPECIFICATIONS AND MATERIAL PROPERTIES OF THE REFERENCE PV MODULE

Layer	Material	Dimension	Density ρ [g/cm³]	Young's modulus E [GPa]	Poisson's ratio ν [-]	CTE α [10^{-6} K^{-1}]
Front glass	soda-lime glass	3.2 mm	2.5*	70*	0.2*	9*
Encapsulant	EVA	400 μm	0.96 [3]	T-dep.†	0.4 [3]	270 [3]
Solar Cell	Cz-Silicon	156.75 mm × 156.75 mm × 0.180 mm	2.329 [3]	Elasticity matrix [3]		T-dep. [20, 21]
Backsheet	TPT	350 μm	2.52 [3]	3.5 [3]	0.29 [3]	50.4 [3]
Frame	aluminium		2.7 [22]	70 [22]	0.33 [22]	23 [22]
Frame-inlay	rubber	8.85 mm × 1.15 mm	0.067*	0.0074*	0.3*	769*

*Provided by manufacturer; †Measured.

the cell edge larger than about 8 mm, the maximum tensile stress is independent of the solder joint length [18]. This implies that for the performed variations—assuming the same metallization layout for all variations—the contribution of the solder joint to the total stress is approximately constant. Therefore, we neglect the ribbons and busbars, which reduce the computational effort significantly. The mesh consists of hexahedral elements with 2700 mesh elements per solar cell and a quadratic serendipity basis function.

The FEM model covers the lamination process, mechanical load (ML), and TC. For the lamination process, the FEM model consists from top to bottom of a glass sheet, encapsulant, solar cells, encapsulant, and backsheet/glass.

For ML and TC, we add an aluminum frame, which is connected to the laminate by a rubber inlay. We simulate the mounting of the framed module on a rack by a fixed constraint on the long side of the module, which is depicted in Fig. 1 and corresponds to model 3 in [19]. The distance to the module edge is 20% of the long side. In the first step, we simulate the lamination process by cooling down from 150 °C to 25 °C. In the second step, we simulate either the homogeneous push load of 2400 Pa or one thermal cycle from +25 °C to −40 °C to +85 °C. To consider the residual stress from lamination, we transfer the stress tensor from the lamination to the ML and TC computation steps. We use linear-elastic and temperature-dependent material models shown in Table I. For the silicon solar cell, we use an anisotropic material model.

The reference is a glass–foil PV module with 60 full-format 156.75 mm × 156.75 mm solar cells and a cell gap of 3 mm. The total size is 1.661 m × 0.997 m. From this reference configuration, we vary the number of solar cells, the cell size, and the cell format independently from each other with the parameters shown in Table II. Additionally, we simulate each configuration as a glass–foil and glass–glass setup. For the glass–glass setup, the backsheet is replaced by glass, with the front and back glass having a thickness of 2 mm. Note that both setups have a frame for a better comparability. The variation of the number of solar cells is composed of an increase of the number of strings (6, 8, 10) per module and an increase of the number of cells per string (10, 12, 14).

We evaluate the FEM simulation results using the principal stresses in the solar cells. During cooling down after lamination, the stronger contraction of the front and back layer compress the solar cells. Hence, the dominating stress is compressive (negative stress values). Consequently, we evaluate the minimum

TABLE II
PV MODULE DESIGN PARAMETERS USED IN THE FEM SIMULATIONS

Glass-foil & glass-glass		
Number of cells	Cell size for 60 cells [mm]	Cell format for 60 cells
60 (6x10)		
72 (6x12)		
84 (6x14)		
80 (8x10)	156.00	full
96 (8x12)	156.75	half
112 (8x14)	161.75	third
100 (10x10)		quarter
120 (10x12)		
140 (10x14)		

The reference parameters are underlined.

stress by using the lowest negative stress value of the third principal stress σ_{III} within the solar cells. The same applies for TC. As a brittle material, silicon solar cells fail under the tensile stress; therefore, compressive stress is not crucial for solar cells. However, independently of the direction, high stresses can lead to delamination [23] and interconnector fatigue [24]. When exposed to ML, the dominating stress in the solar cells is tensile. Therefore, we evaluate the maximum of the first principal stress σ_I within the solar cells. We convert the obtained maximum first principal stress σ_I values from the front and back side of the solar cells into a probability of failure P_f using the Weibull distribution [25] considering the size effect [26]:

$$P_f = 1 - \exp\left(-\sum_i A_{\text{eff},i} \left(\frac{\sigma_{I,\max,\text{ref}}}{\sigma_{0,i}}\right)^{m_i}\right) \quad (1)$$

where A_{eff} is the effective area, $\sigma_{I,\max,\text{ref}}$ is the maximum first principal stress of the reference setup, σ_0 is the Weibull scale factor, and m is the Weibull modulus. The sum is over the values of the front (sunny) and backside, respectively. The effective area A_{eff} can be interpreted as the area of significant stress values and is calculated for the front and backside separately by

$$A_{\text{eff},i} = \int \left(\frac{\sigma_{I,i}(x,y)}{\sigma_{I,\max,\text{ref}}}\right)^m dA_i. \quad (2)$$

The probability of failure P_f expresses the likelihood that within one module at least one crack in at least one solar cell occurs. For the Weibull scale factor σ_0 and modulus m,

TABLE III
WEIBULL PARAMETER USED TO CALCULATE THE PROBABILITY OF FAILURE

Format	Side	Weibull modulus m [-]	Characteristic fracture stress σ_θ [MPa]	Scale factor σ_0 [MPa m²]
full	front	7.8	184	100.8
full	back	6.9	180	91.1
cut	front	8.7	166.4	97
cut	back	17.5	116.1	88.8

Values of Weibull modulus m and characteristic fracture stress σ_θ taken from [27]. Scale factor σ_0 calculated by $\sigma_0 = A_{\text{eff}}^{1/m} \sigma_\theta$, using the effective area 9116 mm² given in [27].
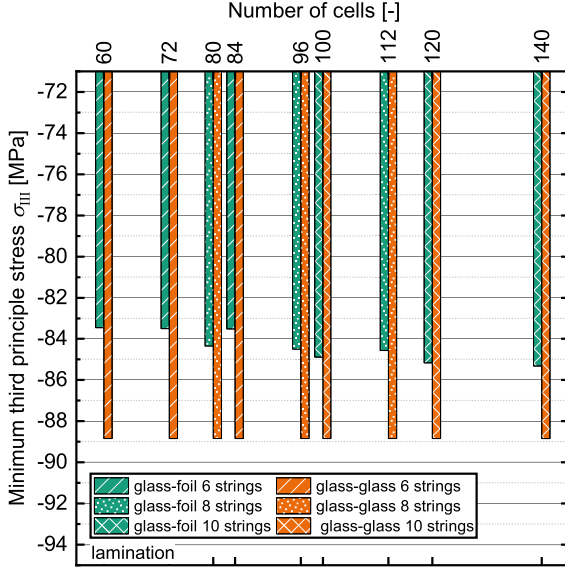
Fig. 2.   Minimum third principal stress σ_{III} of the solar cells after lamination for the variation of the number of solar cells for glass–foil (g-f, green) and glass–glass (g-g, orange) modules. The shading indicates the number of strings per module.

we use values from Kaule *et al*. [27] for full format and cut Al-BSF solar cells, as shown in Table III. In another study, Kaule *et al.* [28] showed that there is no significant difference between Al-BSF and PERC solar cells, as well as between mono- and bifacial PERC solar cells. On the contrary, they found significant differences between different solar cell production processes. Therefore, the presented failure probabilities are just exemplarily and the evaluation has to be performed for a specific cell type individually.

We use the thermal expansion stiffness E_α as a measure of the impact, which the materials have on each other. It is defined as the product of the Young's Modulus E and the coefficient of thermal expansion (CTE) α [29]:

$$E_\alpha = E \cdot \alpha. \tag{3}$$

III. RESULTS

A. Lamination

First, we analyze the variation of the number of cells depicted in Fig. 2. The compressive stress for glass–foil modules increases slightly from 84 MPa (60 cells) to 85 MPa (140 cells). The slight dependence of the cell number originates from the
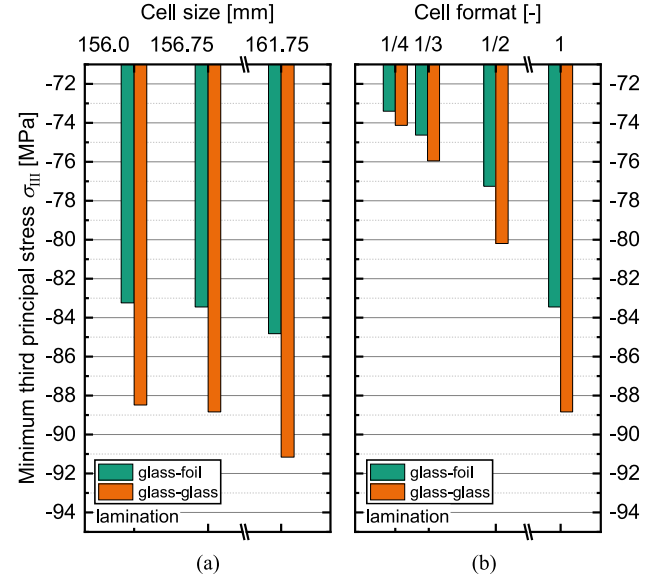
Fig. 3.   Minimum third principal stress σ_{III} of the solar cells after lamination for the variation of the (a) cell size and cell (b) format for glass–foil (green), and glass–glass (orange) modules.

increase in the module size with the number of added cells times the cell gap. Due to the CTE mismatch of the front glass and backsheet, glass–foil modules show a small convex bow after lamination, which adds up to the above-mentioned stress originating from the compression of the solar cells by the front and back layer. Moreover, the bow increases with an increasing module size and hence the stress from the bow. For six strings, the difference is very small and hardly visible in Fig. 2. For an increasing number of strings, the bow becomes more prominent and hence the difference in the compressive stress becomes more significant.

As the glass–glass module stack is vertically symmetric, it does not show a significant bow after lamination and hence there is no dependence on the number of cells. However, it shows a higher compressive stress of 89 MPa compared to the glass-foil setup. This higher compressive stress relates to the higher thermal expansion stiffness E_α of glass as compared with the backsheet. While the glass has a value of 630 kPa/K, the backsheet has a much lower value of 176.4 kPa/K. Additionally, the back-glass is thicker than the backsheet. Consequently, the back glass contracts the solar cell stronger than the backsheet.

Second, we analyze the variation of cell size shown in Fig. 3(a). The compressive stress after lamination in a glass–foil module slightly increases from 83 MPa (156.0 mm) to 85 MPa (161.75 mm). The slight increase originates on the one hand, from the increase of the module size as described above and on the other hand from the larger cell size itself. As the cell is larger, the cell compression by the front and back layer is larger. The latter also applies to glass–glass modules. Consequently, they show a dependence on the cell size, with 89 MPa compressive stress (156.0 mm) to 91 MPa (161.75 mm).

Thirdly, we analyze the variation of cell format depicted in Fig. 3(b). The compressive stress after lamination in a glass–foil module decreases from 83.5 MPa (full format) to 73.4 MPa
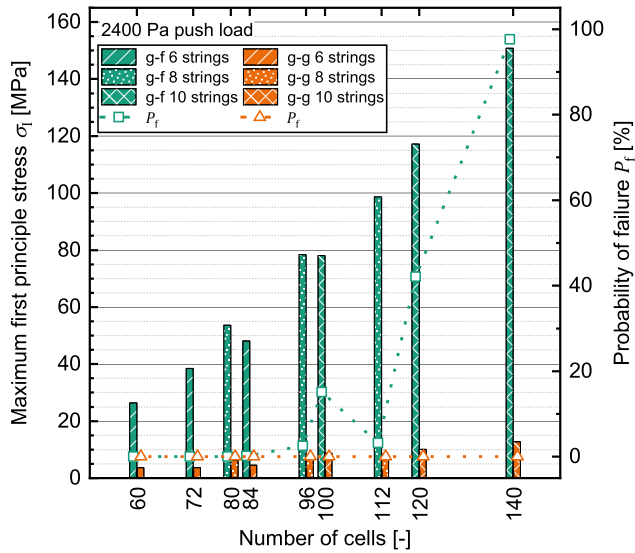
Fig. 4. Maximum first principal stress σ_I at 2400 Pa push load (bars, left axis) with the corresponding probability of failure P_f (symbols, right axis) for the variation of the number of solar cells for glass–foil (g-f, green) and glass–glass (g-g, orange) modules. The shading indicates the number of strings per module.

(quarter cells). The decrease originates from the decrease of the cell length, as described above. The same applies to glass–glass modules. Consequently, they show a dependence on the cell format, with 89 MPa (full format) to 74 MPa (quarter cells). Again due to the higher thermal expansion stiffness E_α, the dependence is stronger.

B. Mechanical Load

First, we analyze the variation of cells number shown in Fig. 4. The dependence of the module size is clearly visible for both glass–foil and glass–glass modules. For glass–foil modules, the tensile stress increases from 26 MPa (60 cells) to 151 MPa (140 cells), which corresponds to a failure probability of 0.00019% (60 cells) and 98% (140 cells). This shows that the mounting has to be adapted for modules with a large area. As shown in a previous publication [30], the chosen mounting structure has a huge influence on the stress in solar cells.

Comparing the different number of strings, *e.g.*, the stress for 80 cells (eight strings with ten cells) and 84 cells (six strings with 14 cells) shown in Fig. 4, shows that adding extra cells to existing strings is more beneficial than adding an extra string. In addition to the stronger change of the aspect ratio, the reason is the mounting on the long side of the module. Adding an extra string increases the width of the module without further support, which changes the deflection and curvature. Furthermore, comparing modules with 96 cells (eight strings with 12 cells) to 100 cells (ten strings with ten cells), as shown in Fig. 4, reveals that a quadratic module shape increases the number of cells with high tensile stress. Both have an almost identical maximum first principal stress σ_I but the more quadratic module with 100 cells has a higher effective area A_{eff} and hence a higher failure probability P_f.

Due to the symmetric setup of glass–glass modules, the solar cells are in the neutral zone [31]. Accordingly, the dominating stress is the residual compressive stress from lamination. The tensile stress is very low with 4 MPa (60 cells) and 13 MPa (140 cells). This corresponds to a negligible probability of failure, as was reported before, *e.g.*, [31], even for the modules with a high number of cells.

Second, we analyze the variation of cell size depicted in Fig. 6(a) for ML. The tensile stress depends on the solar cell size, as the module size increases with the cell size and hence does the deflection. For the glass–foil setup, the tensile stress increases from 26 MPa (156.0 mm) to 32 MPa (161.75 mm). For the glass–glass setup, the tensile stress is 4 MPa and does not increase significantly. All stress values correspond to a negligible probability of failure.

Thirdly, we analyze the variation of cell format shown in Fig. 6(b). The tensile stress in glass–foil modules increases from 26 MPa (full cells) to 33 MPa (quarter cells). The increase originates from the increase in the module size due to additional cell gaps. As the cutting process induces additional flaws in the solar cell, the characteristic fracture stress decreases and the Weibull distribution changes. We use the Weibull parameters of half cells from Kaule *et al.* [27], shown in Table III. All stress values correspond to a negligible probability of failure.

For glass–glass modules, the deflection increases less; hence, the increase in tensile stress is lower. Therefore, a second effect appears: the solar cell follows the deformation of the PV module. Consequently, a cut solar cell with a shorter length is less bowed by the PV module's deflection. Thus, the tensile stress slightly decreases with decreasing cell format. For glass–glass modules, this effect is slightly stronger than the influence of the PV module size, which leads to a very slight decrease of the tensile stress of about 1 MPa.

C. Thermal Cycling

First, we analyze the variation of the cell number depicted in Fig. 7. When cooling down from +25 °C to −40 °C (Fig. 7 top), the solar cells become further compressed by the CTE mismatch, as described above for lamination. In contrast to the lamination process, the laminate is now equipped with a frame. As the aluminum frame has a higher CTE than glass, the module is additionally deformed by this mismatch. Due to the shape of the frame, this bending is opposed to the bending after lamination. As a result, the differences between the different numbers of cells vanish almost completely for both glass–foil and glass–glass modules. This finding disagrees with the results from Kraemer *et al.* [7] that glass–glass modules show no deformation in TC. The discrepancy lies in the different FEM model setups. While Kraemer *et al.* model the frame with a fixed constraint at the outer edges of the module, in this work, the frame is considered in the geometry. This shows the importance of modeling the frame with realistic assumptions, as shown by Schicker *et al.* [19].

When heating up to +85 °C (Fig. 7 bottom), the compression resulting from the CTE mismatch of the front/back layer and silicon reduces. On the contrary, the frame induces a deflection of the PV module, which induces compressive stress in the solar
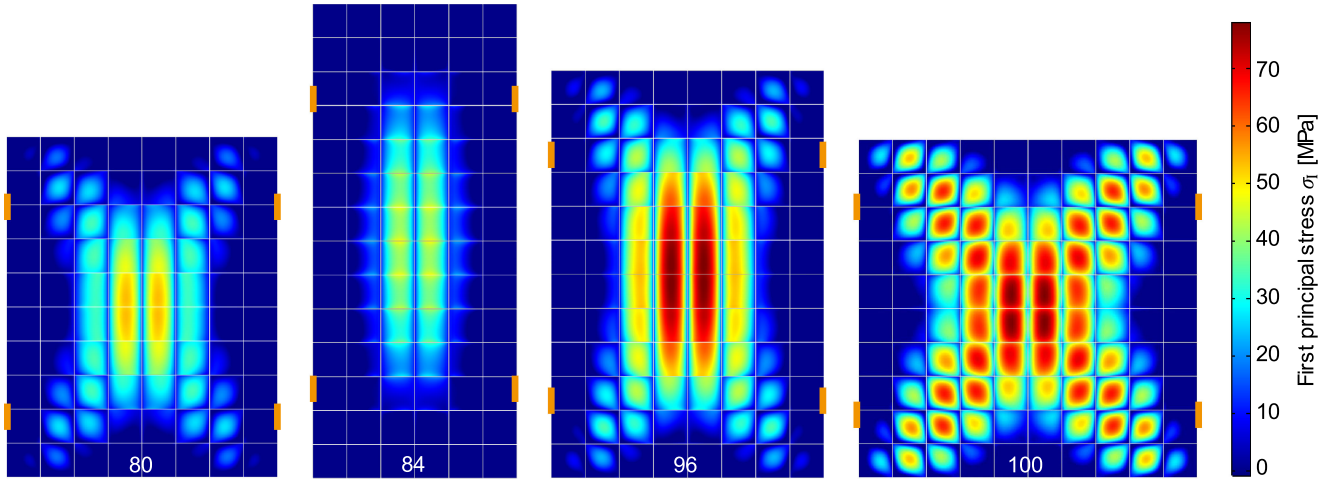
Fig. 5. First principal stress σ_I on the backside of the solar cells for modules with a similar number of cells but a different number of strings. The orange rectangle indicates the position of the frame mounting.
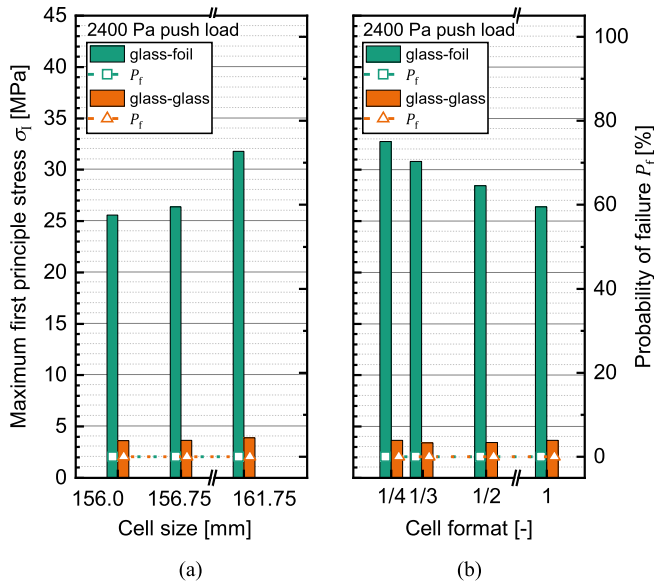
Fig. 6. Maximum first principal stress σ_I at 2400 Pa push load (bars, left axis) with the corresponding probability of failure P_f (symbols, right axis) for the variation of the (a) cell size and (b) cell format for glass–foil (green), and glass–glass (orange) modules.

Fig. 7. Minimum third principal stress σ_III of the solar cells at -40 °C (top) and $+85$ °C (bottom) for the variation of the number of cells for glass–foil (green) and glass–glass (orange) modules.

cells. Increasing the number of cells per string leads to a minimal decrease of the compressive stress. On the contrary, the stress slightly increases for an increase of the number of strings per module from about 78 MPa for 6 strings to about 80 MPa for 10 strings for glass–foil modules. The same is observed for glass–glass modules. However, due to the smaller deformation, the differences are minimal and not significant.

Second, we analyze the variation of cell size shown in Fig. 8. As described above, due to the further compression by the cooling down to -40 °C (Fig. 8 left), the compressive stress increases. Since the frame deformation is opposed to the deformation by the CTE mismatch of glass and backsheet, which increases with the cell size, the increase in cell size leads

to a decrease of compressive stress from 259 MPa (156.00 mm) to 250 MPa (161.75 mm). The same applies to glass–glass modules with a decrease from 268 MPa (156.00 mm) to 258 MPa (161.75 mm).

Heating up to $+85$ °C (Fig. 8 right) again relieves the compressive stress. The opposed deformation by the frame leads to a vanishing difference in cell size for both glass–foil and glass–glass modules with glass–foil modules having a compressive stress of about 79 MPa and glass–glass modules of about 90 MPa.

Thirdly, we analyze the variation of cell format depicted in Fig. 9. As before, the cooling down to -40 °C (Fig. 9 left) further compresses the solar cells. Now, two different effects act
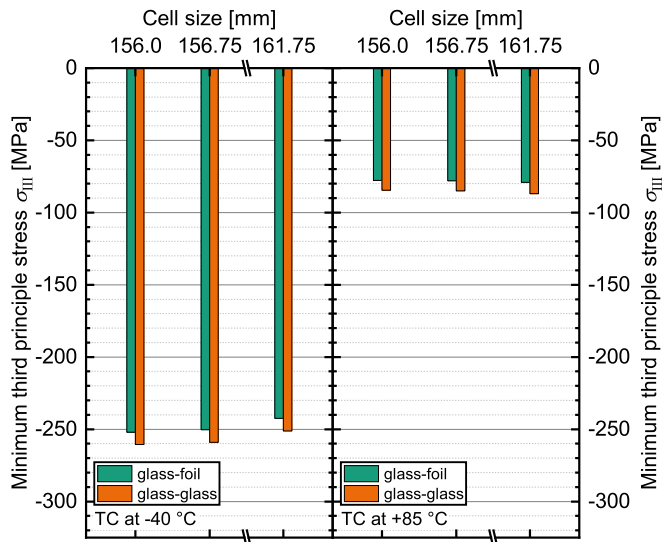
Fig. 8. Minimum third principal stress σ_{III} of the solar cells at $-40\,°C$ (left) and $+85\,°C$ (right) for the variation of the cell size for glass–foil (green) and glass–glass (orange) modules.
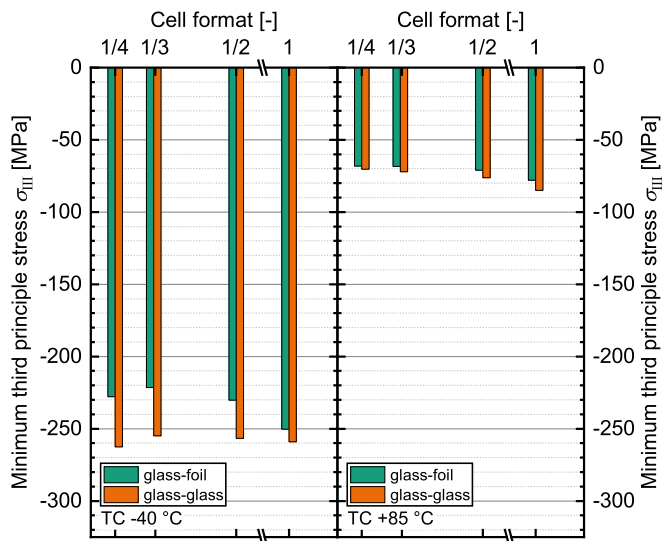
Fig. 9. Minimum third principal stress σ_{III} of the solar cells at $-40\,°C$ (left) and $+85\,°C$ (right) for the variation of the cell format for glass–foil (green) and glass–glass (orange) modules.

against each other. First, as in lamination, a smaller solar cell size leads to a smaller stress build-up. Second, more cell gaps lead to a larger module and consequently, the deformation by the frame becomes lager. Between third cells and quarter cells, the influence of the frame deflection becomes dominating. Therefore, the compressive stress decreases first with a decreasing cell format but then increases again. This is observed for both module setups. For glass–foil modules, the compressive stress values are in the range of 250 MPa (full cells) to 222 MPa (third cells), and for glass–glass: 263 MPa (quarter cells) to 255 MPa (third cells).

When heating up to $+85\,°C$ (Fig. 9 right), the compressive stress is again relieved partially. Also, the deformation due to

the CTE mismatch between glass and frame is in contrast again. However, the induced deformation is smaller than $-40\,°C$. Therefore, the stress relief by the decrease of the cell format is the dominating effect for both module setups. For glass–foil modules, the compressive stress values are in the range of 78 MPa (full cells) to 68 MPa (quarter cells), and for glass–glass: 85 MPa (full cells) to 70 MPa (quarter cells).

IV. CONCLUSION

We present a thorough study of solar cell and PV module dimensions and its effect on the thermomechanical stress on PV modules. The presented FEM simulations cover the lamination process, ML, and TC for glass–foil and glass–glass modules.

The tensile stress from ML of 2400 Pa increases for an increased number of cells per module, as well as for an increase in cell size and when going from full format cells to cut cells. However, all investigated variations have noncritical stress values, except for glass–foil modules with more than 84 solar cells. To prevent cell cracking, the mounting has to be adapted. For glass–glass modules, the stress and the corresponding probability of failure are negligible for all investigated variations. They benefit from the position of the solar cells in the neutral zone, which reduces the stress to negligible values.

Lamination and TC induce compressive stress in the solar cells, which is not responsible for cell cracks but can induce delamination and ribbon fatigue. In TC, the number of solar cells has only a minor effect on the compressive stress. Changing from full format cells to cut cells decreases the compressive stress. Increasing the solar cell size decreases the compressive stress slightly due to the larger module area.

Finally, it can be concluded that increasing the number of cells per string induces less stress than increasing the number of strings per module. The change from 156.00 mm to 161.75 mm solar cells influences the stress of cells in the PV module as well as decreasing the cell format. However, both have a smaller effect than increasing the cell number for example from 60 to 72 cells when considering MLs.

REFERENCES

[1] *International Technology Roadmap for Photovoltaic (ITRPV): 2018 Results*, 10th ed. Frankfurt, Germany: ITRPV, 2019.

[2] M. Köntges, S. Altmann, T. Heimberg, U. Jahn, and K. A. Berger, "Mean degradation rates in PV systems for various kinds of PV module failures," in *Proc. 32nd Eur. Photovol. Sol. Energy Conf. Exhib.*, Munich, Germany, 2016, pp. 1435–1443.

[3] U. Eitner, S. Kajari-Schroeder, M. Köntges, and H. Altenbach, "Thermal stress and strain of solar cells in photovoltaic modules," in *Shell-like Structures: Non-classical Theories and Applications (Advanced Structured Materials)*, vol. 15, H. Altenbach and V. A. Eremeyev, Eds. Berlin, Germany: Springer, 2011.

[4] M. Owen-Bellini, D. Montiel-Chicharro, J. Zhu, T. R. Betts, and R. Gottschalg, "Influence of viscoelastic properties of encapsulation materials on the thermomechanical behavior of photovoltaic modules," *IEEE J. Photovol.*, vol. 8, no. 1, pp. 183–188, Jan. 2018.

[5] M. Owen-Bellini, J. Zhu, T. R. Betts, and R. Gottschalg, "Thermo-mechanical stresses of silicon photovoltaic modules," in *Proc. 13th Photovol. Sci., Appl. Technol. Conf.*, 2017. [Online]. Available: https://repository.lboro.ac.uk/articles/Thermo-mechanical_stresses_of_silicon_photovoltaic_modules/9559487

[6] S. Dietrich, M. Pander, M. Sander, S.-H. Schulze, and M. Ebert, "Mechanical and thermo-mechanical assessment of encapsulated solar cells by finite-element-simulation," in *Proc. SPIE Sol. Energy Technol.*, San Diego, CA, USA, vol. 77730F, 2010. [Online]. Available: https://www.spiedigitallibrary.org/conference-proceedings-of-spie/7773/1/Mechanical-and-thermomechanical-assessment-of-encapsulated-solar-cells-by-finite/10.1117/12.860661.short?SSO=1

[7] F. Kraemer and S. Wiese, "Assessment of long term reliability of photovoltaic glass–glass modules vs. glass-back sheet modules subjected to temperature cycles by FE-analysis," *Microelectron. Rel.*, vol. 55, no. 5, pp. 716–721, 2015.

[8] U. Eitner, M. Köntges, and R. Brendel, "Use of digital image correlation technique to determine thermomechanical deformations in photovoltaic laminates: Measurements and accuracy," *Sol. Energ. Mat. Sol. C.*, vol. 94, no. 8, pp. 1346–1351, 2010.

[9] U. Eitner, S. Kajari-Schroeder, M. Köntges, and R. Brendel, "Non-linear mechanical properties of ethylene-vinyl acetate (EVA) and its relevance to thermomechanics of photovoltaic modules," in *Proc. 5th World Conf. Energy Convers.*, Valencia, Spain, 2010, pp. 4366–4368.

[10] S. K. Tippabhotla et al., "Thermomechanical residual stress evaluation in multi-crystalline silicon solar cells of photovoltaic modules with different encapsulation polymers using synchrotron X-ray microdiffraction," *Sol. Energ. Mat. Sol. C.*, vol. 193, pp. 387–402, 2019.

[11] X. Meng et al., "Quantitative mapping of deflection and stress on encapsulated silicon solar cells," *IEEE J. Photovol.*, vol. 8, no. 1, pp. 189–195, Jan. 2018.

[12] A. J. Beinert et al., "Enabling the measurement of thermomechanical stress in solar cells and PV modules by confocal micro-Raman spectroscopy," *Sol. Energ. Mat. Sol. C.*, vol. 193, pp. 351–360, 2019.

[13] *Terrestrial Photovoltaic (PV) Modules – Design Qualification and Type Approval—Part 2: Test Procedures*, IEC 61215-2:2016, 2016.

[14] A. J. Beinert et al., "Thermomechanical evaluation of new PV module designs by FEM simulations," in *Proc. 36th Eur. Photovol. Sol. Energy Conf. Exhib.*, Marseille, France, 2019, pp. 783–788.

[15] A. J. Beinert et al., "Stress mapping by confocal Raman spectroscopy on solar cells and modules," in *Proc. 7th World Conf. Photovol. Energy Convers.*, Waikoloa Village, HI, USA, 2018, pp. 3613–3617.

[16] A. J. Beinert, R. Leidl, P. Sommeling, U. Eitner, and J. Aktaa, "FEM-based development of novel back-contact PV modules with ultra-thin solar cells," in *Proc. 33rd Eur. Photovol. Sol. Energy Conf. Exhib.*, Amsterdam, The Netherlands, 2017, pp. 42–47.

[17] S. Dietrich, "Numerische untersuchungen zur mechanischen zuverlässigkeit verkapselter siliziumsolarzellen," Dissertation, *Fakultät für Maschinenbau*, Halle (Saale): Otto-von-Guericke-Universität Magdeburg, 2014.

[18] L. C. Rendler et al., "Thermomechanical stress in solar cells: Contact pad modeling and reliability analysis," *Sol. Energ. Mat. Sol. C.*, vol. 196, pp. 167–177, 2019.

[19] J. Schicker, C. Hirschl, and R. Leidl, "Effect of PV module frame boundaries on stresses in solar cells," *J. Energ. Challenges Mech.*, vol. 1, no. 3, pp. 155–162, 2014.

[20] R. B. Roberts, "Thermal expansion reference data: Silicon 80-280K," *J. Phys. D: Appl. Phys.*, vol. 15, no. 9, pp. L119–L120, 1982.

[21] R. B. Roberts, "Thermal expansion reference data: Silicon 300-850 K," *J. Phys. D: Appl. Phys.*, vol. 14, no. 10, pp. L163–L166, 1981.

[22] W. M. Haynes, Ed., *CRC Handbook of Chemistry and Physics*. Boca Raton, FL, USA: CRC Press, 2014.

[23] M. Knausz et al., "Thermal expansion behavior of solar cell encapsulation materials," *Polym. Testing*, vol. 44, pp. 160–167, 2015.

[24] S. Wiese, R. Meier, and F. Kraemer, "Mechanical behaviour and fatigue of copper ribbons used as solar cell interconnectors," in *Proc. 11th IEEE Int. Conf. Thermal, Mech. Multi-Phys. Simul. Experiments Microelectron. Microsyst.*, Bordeaux, France, 2010, pp. 1–5.

[25] W. Weibull, *A Statistical Theory of the Strength of Materials*. Stockholm, Sweden: Generalstabens Litografiska Anstalts Förlag, 1939.

[26] D. Munz and T. Fett, *Ceramics: Mechanical Properties, Failure Behaviour, Materials Selection*, 1st ed. Berlin, Germany: Springer, 2001.

[27] F. Kaule et al., "Mechanical damage of half-cell cutting technologies in solar cells and module laminates," in *Proc. AIP Conf.*, 2018, vol. 1999, pp. 020013-1–020013-9.

[28] F. Kaule, S. Meyer, and S. Schönfelder, "Benchmarking mechanical strength data for new solar cell concepts," in *Proc. 33rd Eur. Photovol. Solar Energy Conf. Exhib.*, Amsterdam, The Netherlands, 2017, pp. 276–279.

[29] W. Carroll, E. Cuddihy, and M. Salama, "Material and design considerations of encapsulants for photovoltaic arrays in terrestrial applications," in *Proc. 12th IEEE Photovol. Spec. Conf.*, 1976, pp. 332–339.

[30] A. J. Beinert, M. Ebert, U. Eitner, and J. Aktaa, "Influence of photovoltaic module mounting systems on the thermo-mechanical stresses in solar cells by FEM modelling," in *Proc. 32nd Eur. Photovol. Sol. Energy Conf. Exhib.*, Munich, Germany, 2016, pp. 1833–1836.

[31] A. M. Gabor et al., "Mechanical load testing of solar panels—Beyond certification testing," in *Proc. 43rd IEEE Photovol. Spec. Conf.*, Portland, OR, USA, 2016, pp. 3574–3579.

Andreas J. Beinert received the Master degree in physics from the Albert Ludwig University of Freiburg, Freiburg, Germany, in 2014. Since July 2015, he has been currently working toward the Ph.D. degree with the Karlsruhe Institute of Technology, Karlsruhe, Germany.

He is also associated with the Fraunhofer Institute for Solar Energy Systems ISE, Freiburg, Germany, where he is involved in the research on the thermomechanics of PV modules. His research interests include thermomechanical FEM analysis of PV modules, stress measurement techniques, and material characterization.

Pascal Romer received the Master degree in physics from thet Albert Ludwig University of Freiburg, Freiburg, Germany, in 2019.

He joined the group "PV Module Technology" at the Fraunhofer Institute for Solar Energy Systems ISE, Freiburg, Germany, in 2014. His research interests include the thermomechanical FEM analyses of PV modules and stress measurement techniques.

Martin Heinrich received the Ph.D. degree from the National University of Singapore, Singapore, in 2015.

He was with SERIS for two years and with the Fraunhofer Institute for Solar Energy Systems ISE, Freiburg, Germany, for two years. As a Group Leader with the University of Freiburg, he was focusing on solar cell engineering and a Coordinator of the online study program "Solar Energy Engineering." He joined the Department of Module Technology, Fraunhofer Institute for Solar Energy Systems ISE, in 2017, where he is currently a Coordinator for the topic PV for mobility.

Max Mittag received the Diploma in industrial engineering and management from the Freiberg University of Mining and Technology, Freiberg, Germany, in 2010.

In 2010, he joined the Department "PV Module Technology" at the Fraunhofer Institute for Solar Energy Systems ISE, Freiburg, Germany, and developed novel module concepts. He is currently the Head of the team "Module Simulation." His research interests include cell-to-module efficiency analysis, techno-economical assessments as well as electrical, optical, thermal, or other simulations.

Jarir Aktaa received the Ph.D. degree from the University of Karlsruhe, Karlsruhe, Germany, in 1994, and the Habilitation from the Karlsruhe Institute of Technology (KIT), Karlsruhe, in 2009.

Since 1996, he has been the Head of Department "Mechanics of Materials 2," Institute for Applied Materials – Materials and Biomechanics, KIT, leading numerous R&D projects on the characterization, modeling and simulation of highly loaded materials and components. He is also a Professor for mechanics of materials with KIT.

Dirk Holger Neuhaus received the Ph.D. degree from the University of New South Wales, Sydney, NSW, Australia.

He was a Development Engineer with Pacific Solar Pty Ltd. He was with Solarworld AG for more than 15 years, initially responsible for quality assurance and technology in cell production, later heading the global R&D activities along the entire value chain. In 2018, he joined the Fraunhofer Institute for Solar Energy Systems ISE, Freiburg, Germany, where he is currently In-Charge of Module Technology.